PAN ARCHIVES OF ACOUSTICS
Vol. **39**, No. 2, pp. 249–260 (2014)

DOI: 10.2478/aoa-2014-0029

A Numerical Approach to Calculate the Radiation Efficiency of Baffled Planar Structures Using the Far Field

Mario A. GONZÁLEZ-MONTENEGRO[(1)], Roberto JORDAN[(1)], Arcanjo LENZI[(1)], Jorge P. ARENAS[(2)]

[(1)] *Federal University of Santa Catarina, Department of Mechanical Engineering*
Campus Trindade, Florianópolis, Brazil; e-mail: mario.gonzalez@lva.ufsc.br

[(2)] *Institute of Acoustics, Univ. Austral de Chile*
PO Box 567, Valdivia, Chile

(*received May 20, 2013; accepted June 4, 2014*)

A numerical method is developed for estimating the acoustic power of any baffled planar structure, which is vibrating with arbitrary surface velocity profile. It is well known that this parameter may be calculated with good accuracy using near field data, in terms of an impedance matrix, which is generated by the discretization of the vibrating surface into a number of elementary radiators. Thus, the sound pressure field on the structure surface can be determined by a combination of the matrix and the volume velocity vector. Then, the sound power can be estimated through integration of the acoustic intensity over a closed surface. On the other hand, few works exist in which the calculation is done in the far field from near field data by the use of radiation matrices, possibly because the numerical integration becomes complicated and expensive due to large variations of directivity of the source. In this work a different approach is used, based in the so-called Propagating Matrix, which is useful for calculating the sound pressure of an arbitrary number of points into free space, and it can be employed to estimate the sound power by integrating over a finite number of pressure points over a hemispherical surface surrounding the vibrating structure. Through numerical analysis, the advantages/disadvantages of the current method are investigated, when compared with numerical methods based on near field data. A flexible rectangular baffled panel is considered, where the normal velocity profile is previously calculated using a commercial finite element software. However, the method can easily be extended to any arbitrary shape. Good results are obtained in the low frequency range showing high computational performance of the method. Moreover, strategies are proposed to improve the performance of the method in terms of both computational cost and speed.

Keywords: propagating matrix, far field, sound power, structural finite element analysis.

1. Introduction

Sound radiation from baffled planar sources is important in many areas of engineering where noise control is required. Particularly, the sound power is a suitable parameter to characterize the strength of the sound generated by a vibrating structure. The fundamentals of acoustic radiation analysis of vibrating baffled planar bodies were established two centuries ago by Lord Rayleigh, through the well-know Rayleigh integral (Rayleigh, 1896), which relates the acoustic pressure at an arbitrary point of observation in the propagation media to the distribution of out-of-plane velocity on the structure. Analytical solutions are possible for simple geometries (Wallace, 1972). This is an useful feature to find analytical expressions of the displacement vibrating field and, consequently, the sound power. However, in many cases the vibrating flat body has either a complex geometry or regular geometry and complicated out-of-plane velocity field. In such cases the Rayleigh Integral is difficult or impossible to solve analytically and numerical methods are the only choice. In this case, the vibrating field may be represented as a discrete velocity field or well as a finite set of planar acoustic radiators with a specific velocity amplitude.

On the other hand, it is possible to distinguish two ways for the sound power calculation: using the near sound pressure field or using the far field, where the sound pressure is calculated from the vibration field data. The literature indicates that there are more approaches using the former. In this case the integration domain is the structure surface. Numerical evaluation of the Rayleigh Integral is possible as reported by Sandman (1977). However, several more efficiently solutions have been developed. Williams and Maynard (1982) developed a wave number representation of the Rayleigh Integral which is solved through the fast Fourier transform algorithm, allowing a 400 times computational speed increase, when compared to direct numerical integration. In this case, the discretization domain features must satisfy proper conditions to guarantee the application of the Discrete Fourier Transform over the velocity vibration function. Fiates (2003) used the same approach to investigate the radiation efficiency of stiffened panels modeled with finite elements.

A more recently work of this kind was developed by Langley (2007), who considered both wave number representation and impedance matrix formulation, where the acoustic pressure is expressed in terms of wavelets. The discretization domain may also be useful to consider directly each sub-region as a small acoustic radiator, and thus, the whole structure as a finite set of elementary radiators. This point of view was introduced simultaneously by Mollo and Bernhard (1989), Borgiotti (1990) and Cunefare and Koopmann (1991). In this case, the pressure at any point of the structure is also calculated by a summation of all contributions, but in a matrix form, in terms of a combination of an *impedance matrix* and a volume velocity vector.

So, both the Williams-Maynard's approach as the Impedance Matrix approach are suitable to import the normal velocity data from structural finite element models, and they have interesting advantages. For example, the method based on the Fourier transform can be very fast only under the condition that the number of elements is a power of two. In the case of regular mesh this is easy to achieve, however, complex structures with more detail often require irregular mesh and therefore, the number of elements becomes difficult to controlling.

On the other hand, the method based on the impedance matrix also offers advantages: for example, due to the reciprocity principle, the matrix $[Z]$ is always symmetric, and this useful feature can be combined with linear algebraic techniques. In that sense, Fahy (Fahy, Gardonio, 2007) notes that in the symmetrical case it is always possible to separate the diagonal and off-diagonal terms of the impedance matrix for any shape of baffled flat panel, allowing to express the sound radiation in terms of modes that radiate independently. This property was useful to Baumann, Ho and Robertshaw (1992), Elliott and Johnson (1993) and Borgiotti and Jones (1994) to develop the useful and well-known concept of *radiation filters* to be applied in the active control of radiated sound power. Moreover, the quadratic nature of W_{rad} has been considered by Mollo and Bernhard (1989), Naghshineh *et al.* (1992), Naghshineh and Koopmann (1993), and more recently by Fisher *et al.* (2012) to be applied in quadratic optimization theory to minimize the acoustic radiated power. In that sense, Naghshineh and Koopmann (1993) considered localized forces (actuators) in the vibrating structure to explore the control mechanisms.

It should be noted that for the calculation of sound power, either by velocity field based methods (such as Williams-Maynard's Method (Williams, Maynard, 1982)) or by the Matrix Impedance Method, it is always considered the sound pressure at the vibrating surface. Mathematically, it means that the sound power is calculated from two double integrals, one nested on the other, with the same integration domain. In fact, some authors had reported formulations using quadruple integrals (Naghshineh, Koopmann, 1992; Atalla, Nicolas, 1994; Li, 2006; Langley, 2007; Fahy, Gardonio, 2007). In general, this feature can lead to an expensive computational effort when considering a large number of elements. In that sense, it is interesting to ask whether it is possible to use two different integration domains. This could be useful to reduce the computational cost associated with the calculation of sound power. One way to do that is to consider another different surface outside the vibrating surface and the sound pressure to any point located on that new domain. Indeed, few works have been found in the literature related to this idea and using radiation matrices, like the radiation impedance matrix $[Z]$.

Atalla and Nicolas (1994) compared several models used to evaluate the radiation efficiency of plate-like radiators, included radiation impedance matrix techniques. Moreover, the authors investigated about both near field and far field approaches. In the later is introduced a method developed by Berry (1991), who employed the two-dimensional Fourier transform approach over a hemisphere of infinite radius to integrate the radial acoustic intensity in the far field. Berkhoff (2002), used a cost function associated to sound power in the far field to minimize it in terms of time-averaged squared pressure data, considering a large distance from the structure and using a sufficient number of measurement positions. Zou and Crocker (2009) derived an equation for calculating the sound power radiated from a rectangular plate with arbitrary boundary conditions, in which the sound power radiated from the plate is rep-

resented in terms of the normal velocity distribution on the plate and a coupling matrix, by integrating the sound intensity over a hemisphere in the far field. PÀMIES *et al.* (2011) estimate the sound power radiated by an aperture placed in an enclosure wall to low frequencies by adding the sound intensity over a hemisphere of fixed radius surrounding the aperture. So, these researches suggest to use an hemispherical surface in the far field, like as the standardized method ISO 3745 (2003) to measure the sound power of a sound source. However, ATALLA and NICOLAS (1994) consider that far field approaches could be more computational expensive than near field ones, mainly at middle and high frequencies, due to large variations of directivity of the source. In that sense, it would be interesting to found some strategy for using the far field approach and this idea is the main focus of this paper.

In regard to the analysis of sound radiation of vibrating structures by means of matrix methods, it could be cited the work of FAN *et al.* (1997) who modeled the sound field of a single-source ultrasound transducer as composed of many small elements, where the sound pressure vector, that represents the acoustic far field, is calculated in terms of a matrix $[H]$, similar to $[Z]$, but different since it is a relationship between the far field acoustic pressure vector and the normal velocity vector of the source. BAI and TSAO (2002) used the same matrix technique to analyze the acoustic radiation of baffled planar sources, and called such matrix as *propagating matrix*. ARENAS *et al.* (2010) also use the propagating matrix $[G]$ and a singular value decomposition to estimate the directivity pattern from a vibrating baffled elliptical piston and considering the radiation of each element as an equivalent circular piston.

The approach proposed here differs from previous works because the sound power of a baffled planar vibrating structure is calculated using the far field, by means of the Propagating Matrix $[G]$: since the velocity vibrating field is previously known, it is possible to determine the acoustic pressure of a set of points over an hemispherical surface and integrate the acoustic intensity over this domain, as indicated in the standardized method ISO 3745 (2003). Through numerical analysis, the advantages/disadvantages of the current method are investigated, when compared with numerical methods based in near field data. A flexible rectangular baffled panel is considered, where the normal velocity profile is calculated using the finite element software ANSYS. After that, the velocity field was used as a input data to the current approach implemented in MATLAB. So, the method can easily be extended to an arbitrary shape. Moreover, strategies are proposed to improve the performance of the method in terms of both computational cost and speed.

2. Theory

The sound radiated from a flat panel (rigid or flexible) depends strongly on the coupling between the vibrating surface and the surrounding fluid. When the structure is vibrating, the particles of fluid very close to the body also vibrate, generating acoustic waves. Consider a baffled flat panel of rectangular shape whose surface is located in the $x-y$ plane, centered at the origin of the coordinate system which is radiating acoustic waves into a fluid in the half space $z > 0$, as indicated in Fig. 1. Let the panel be divided into N elements of area A_e, with $e = 1, 2, \ldots, N$. Thus, the vibration profile can be specified in terms of the elementary normal velocity v_e at their center positions. Assuming that the characteristic size of the elements is small compared with both the structural wavelength and the acoustic wavelength, the pressure at M points in the acoustic medium can be represented by a linear transformation of the volume velocity vectors $A_e v_e$ through a propagating matrix operator $[G]$, defined by:

$$\begin{aligned} \{p\} &= [G]\,\{v\}, \\ G_{rs} &= \frac{j\omega\rho_0 A_e e^{-jkR_{rs}}}{2\pi R_{rs}}, \end{aligned} \tag{1}$$

where

$$\{p\} = [p_1, p_2, \cdots, p_M]^{\mathrm{T}}$$

and

$$\{v\} = [v_1, v_2, \cdots, v_N]^{\mathrm{T}}$$

are the sound pressure and normal velocity vectors, R_{rs} is the distance between the center of the r-th element and the s-th point in the far field, ω is the circular frequency and ρ_0 is the density of the fluid. Now, consider that the M field points are distributed into an hemispherical surface surrounding the vibrating body, with center at the origin of the coordinate system as indicated in Fig. 2. In general, the choice of location of the points is arbitrary. However, we will consider the

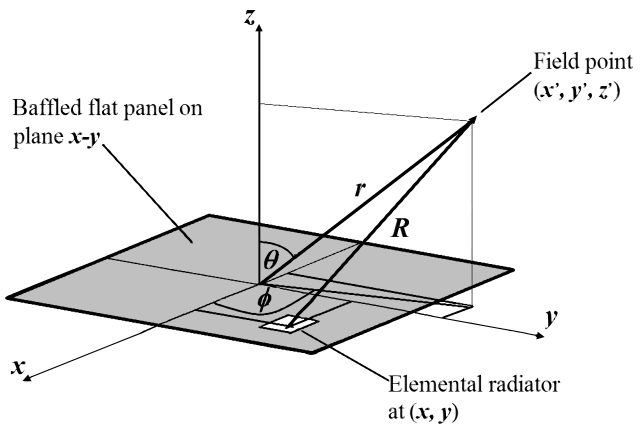

Fig. 1. Geometry of rectangular baffled flat panel.

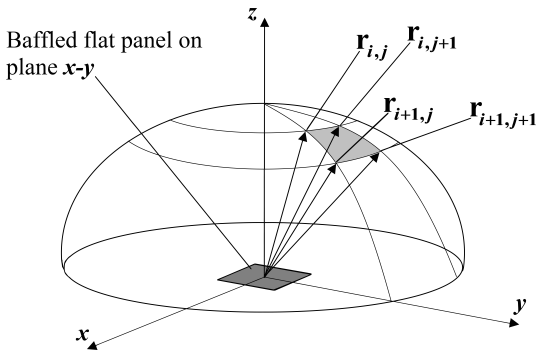

Fig. 2. Geometry of a hemispherical surface surrounding the source.

following regular partition to the spherical coordinates θ and ϕ:

$$\begin{aligned} \Theta &= \{\theta_i \in [0, \pi/2] \mid \theta_i = \theta_{i-1} + \Delta\theta, \\ &\quad \text{and} \quad i = 1, \cdots, M_\theta\}, \\ \Phi &= \{\phi_j \in [0, 2\pi] \mid \phi_j = \phi_{j-1} + \Delta\phi, \\ &\quad \text{and} \quad j = 1, \cdots, M_\phi\}, \end{aligned} \tag{2}$$

where M_θ and M_ϕ are integer positive numbers such as:

$$M = M_\theta M_\phi, \tag{3}$$

and $\mathbf{r}_{i,j}$ is a vector with the spherical coordinates to any point in the hemispherical surface defined by Eq. (2), such that:

$$\mathbf{r}_{i,j} = (\theta_i, \phi_j, r), \quad \text{with} \quad |\mathbf{r}_{i,j}| = r. \tag{4}$$

Now $p_{i,j}$, $p_{i,j+1}$, $p_{i+1,j}$ and $p_{i+1,j+1}$ are the sound pressure at positions $\mathbf{r}_{i,j}$, $\mathbf{r}_{i,j+1}$, $\mathbf{r}_{i+1,j}$ and $\mathbf{r}_{i+1,j+1}$, respectively. In addition, let $\Delta A_{i,j}$ be the area of the hemispherical region among those points, defined by:

$$\Delta A_{i,j} = r^2 \sin\theta \Delta\theta \Delta\phi. \tag{5}$$

To estimate the sound power, we can consider the sound intensity for each $\Delta A_{i,j}$, in a similar way that the standardized method ISO 3745 (2003). In that sense, we can use the following spatial average of sound pressure:

$$\langle p^2 \rangle_{\Delta A_{i,j}} = \frac{p_{i,j}^2 + p_{i,j+1}^2 + p_{i+1,j}^2 + p_{i+1,j+1}^2}{4}, \tag{6}$$

and the well-know expression for the sound intensity in the far field (Wallace, 1972; Fahy, Gardonio, 2007):

$$I_{\Delta A_{i,j}} = \frac{\langle p^2 \rangle_{\Delta A_{i,j}}}{\rho_0 c}, \tag{7}$$

where c is the speed of sound.

The following expression of sound power is obtained by combination of Eqs. (5), (6) and (7):

$$W_{\text{rad}} = \sum_{i=1}^{M_\theta - 1} \sum_{j=1}^{M_\phi - 1} I_{\Delta A_{i,j}} \Delta A_{i,j}. \tag{8}$$

3. Numerical results

In order to verify the effectiveness of the proposed method, in what follows it will be considered a vibrating flexible plate with a rectangular shape and mounted flush into a rigid infinite baffle. This kind of geometry and boundary conditions are suitable to compare the results of this work with some analytical and numerical models found in the literature.

When the panel is vibrating, the largest amount of energy is concentrated at the natural frequencies of the structure (Fiates, 2003). Taking this fact into consideration it is possible to obtain the velocity profile of each mode shape by using localized excitation at natural frequencies. This kind of analysis can be applied to either experimental tests or numerical models such as finite elements. However, in the last case the same results may be obtained by using numerical modal analysis. This option is computationally less expensive and faster in terms of CPU time than the former and it will be used in this work. The parameters of the plate are: area $= 1.0 \times 0.8$ m^2, thickness $h = 7$ mm, Young's modulus $E = 210$ GPa, density $\rho = 7860$ kg/m^3, and Poisson ratio $\nu = 0.33$. The plate is the same used by Fiates (2003), who investigated the radiation efficiency of stiffened panels. In the same research, several structures were modeled with FEM and the sound radiation was estimated by using the algorithm developed by Williams and Maynard (1982). In this work, the structure described above is modeled by using the Finite Element software ANSYS. The modal analysis option was used to obtain the normal velocity distribution of each mode shape.

The procedure to calculate the normal velocity is described in Fig. 3. To ensure a good comparison the same mesh used in Fiates's research was employed: the structure was modeled by using a regular mesh with quadrilateral shell elements, each one having four nodes. A total of 3969 elements and 4096 nodes were used. In that case it was important the choice of a number of nodes equal to a power of two because Fiates used the Williams-Maynard's Method which is based

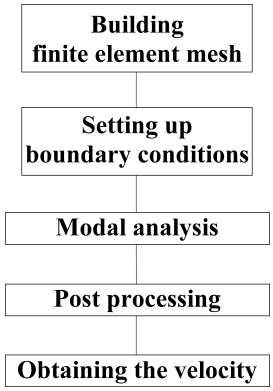

Fig. 3. Numerical determination of normal velocity.

in the spatial two-dimensional Fast Fourier Transform of the velocity vibration function. The normal velocity information is also important to estimate the vibrating energy of the structure. In that sense, the *sound radiation efficiency*, σ_{rad}, is a suitable parameter to describe the effectiveness of any vibrating structure to radiate sound energy and is defined by (Wallace, 1972; Fahy, Gardonio, 2007):

$$\sigma_{\text{rad}} = \frac{W_{\text{rad}}}{\rho_0 c S \left\langle \overline{v}^2 \right\rangle}, \tag{9}$$

where $\left\langle \overline{v}^2 \right\rangle$ is the average mean-square velocity and S represents the area of the panel.

The radiation efficiency may be seen as a measure of the sound radiation in dependence of the geometry of the panel, because is equivalent to a normalized sound power with respect to the specific acoustic impedance of the surrounding media, the area and vibrating normal velocity of the source. Indeed, this parameter depends strongly of the mode shape, as reported by Wallace (1972).

In Fig. 4 it is shown the curve σ_{rad} as a function of frequency, for the structure defined above. Fiates (2003) estimates this parameter using the method developed by Williams and Maynard (1982), which has been compared with a previous theoretical model given by Maidanik (1962). That is a very efficient approach so that we can be sure about the reliability of the results. On the other hand, Fig. 5 presents σ_{rad} for the same structure and boundary conditions, but calculated with the current method developed in this work. Because this approach is based on the calculation of the sound intensity in the far field, it is important to use an hemispherical surface large enough to ensure plane wavefronts in the vicinity of the hemisphere (shown in Fig. 2), where the sound pressure is calculated. This is absolutely necessary for making use of Eq. (7). Thus, it should be clear that the calculation of σ_{rad} by using this approach is sensitive to the radius of the hemispherical surface.

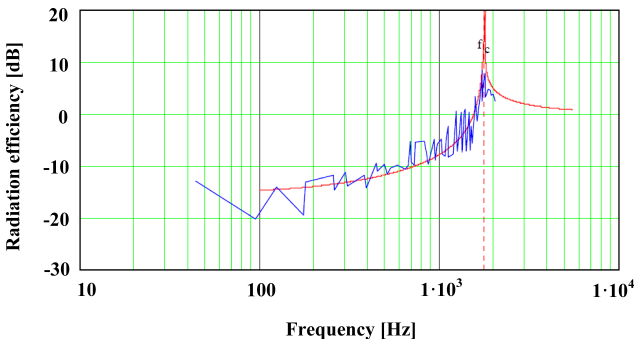

Fig. 4. Radiation efficiency calculated by Fiates (2003) (blue line), and the theoretical model developed by Maidanik (1962) (red line). The dotted line indicates the coincidence frequency.

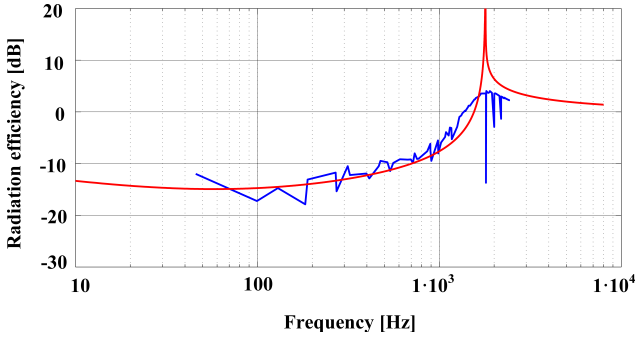

Fig. 5. Radiation efficiency calculated by the current method (blue line), and the theoretical model developed by Maidanik (1962) (red line).

In order to quantify the sensitivity of σ_{rad} with the radius of the hemisphere, a new simulation was performed for the same structure. This time, the maximum frequency analyzed was 4819 Hz. A total of 8000 elements and 8181 nodes were used to ensure compliance with the criterion of twelve elements for each flexural wavelength. In Figs. 6 and 7 it is shown a family of curves of σ_{rad} for several values of the radius of the hemisphere. It should be noted that σ_{rad} is too sensitive at middle and high frequencies, while it remains unchanged at low frequencies. Moreover, we can see

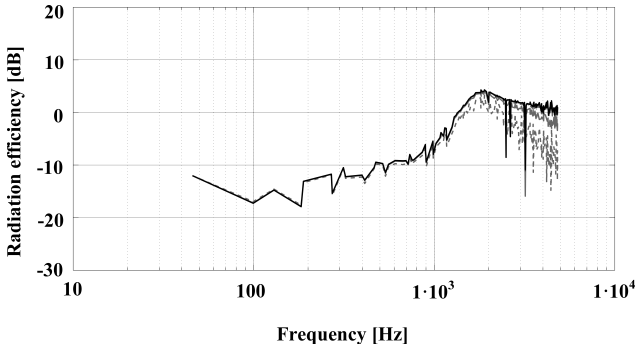

Fig. 6. Radiation efficiency calculated for several values of radius of the hemisphere.

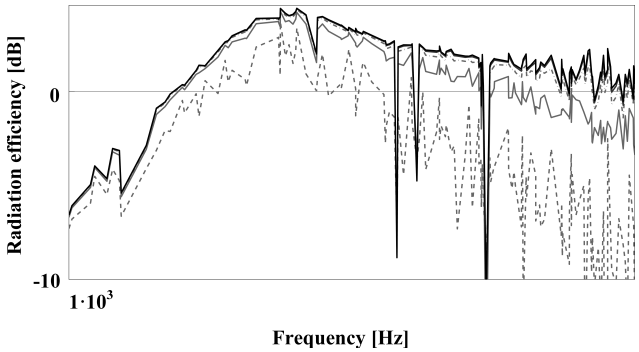

Fig. 7. Radiation efficiency calculated for several values of radius of the hemisphere: 2 m ——— , 5 m ——— , 10 m ——·——·—— , 20 m ——— , 30 m . . . . , 60 m ——— (Detail of Fig.6).

that for a radius greater than 30 m, no changes are observed in the frequency range. However, it is important to determine quantitatively a suitable value of the radius that may be used with confidence in the following analysis. One way to do this is by defining an error ratio between two different $\sigma_{\rm rad}$ curves for two different values of radius as follows:

$$\varepsilon_{\rm radius} = \frac{\sum_{j=1}^{N_{\rm freq}} |\sigma_{\rm rad}(f, r_{{\rm hemisph},i+1}) - \sigma_{\rm rad}(f, r_{{\rm hemisph},i})|}{\sum_{j=1}^{N_{\rm freq}} \sigma_{\rm rad}(f, r_{{\rm hemisph},i})}, \quad (10)$$

where $r_{{\rm hemisph},i}$ is the i-th radius of the hemisphere and $N_{\rm freq}$ is the number of structural natural frequencies. This analysis considered up to the first 170 natural frequencies.

In Fig. 8 it is possible to observe the convergence error rate of the radiation efficiency as a function of the hemispherical radius. For $r_{\rm hemisph} = 2$ m, the error rate is approximately 40%, while for a radius of 30 m the same is less than 0.1%. Thus, $r_{\rm hemisph} = 30$ m may be considered as quite reliable so that this information will be used in the following analysis.

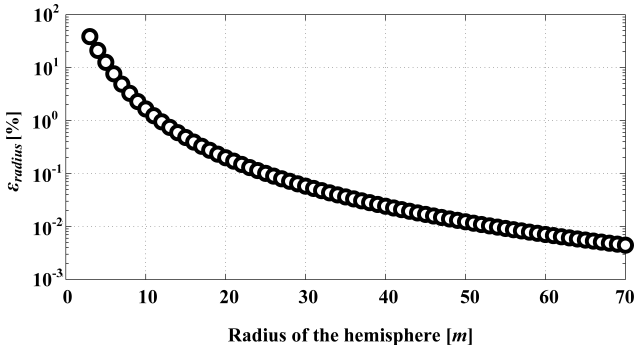

Fig. 8. Convergence error rate (log scale) of radiation efficiency with hemispherical radius.

4. The mesh of the hemispherical surface

Until now, it was discussed the discretization of the vibrating surface (by using FEM). However, nothing has been said about the discretization of the hemispherical surface. From Eq. (8), it is possible to note that the hemisphere is divided into $(M_\theta - 1)(M_\phi - 1)$ small regions. Because there is no information about the effects of such discretization in the radiation efficiency, it is absolutely necessary to make a proper analysis that allow us to understand the advantages and limitations of this approach. In Fig. 9, it is shown a set of radiation efficiency curves considering different values of the hemispherical surface parameter M, defined in Eq. (3). Particularly, we shall consider that

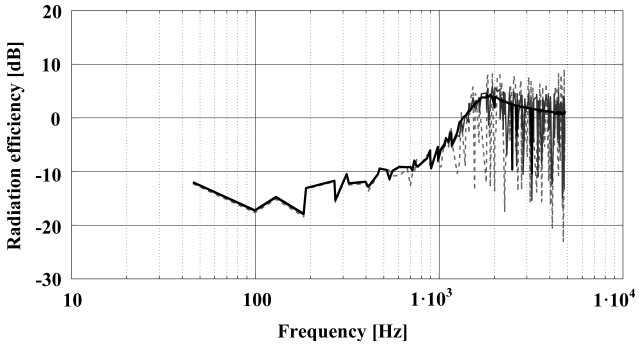

Fig. 9. Radiation efficiency calculated for several values of the parameter M: $M' = 10$, $M' = 20$, $M' = 50$.

$M_\theta = M_\phi = M'$, so that $M = M'^2$. Thus, one can see that for small values of $M'(M' = 10)$, there is considerable error in the calculated radiation efficiency in middle and high frequencies, which distorts the expected typical nature of $\sigma_{\rm rad}$, particularly at frequencies near and above the coincidence frequency. However, the same error can be reduced by increasing M'. In fact, for $M' = 50$ small distortions are observable and the curve presents the asymptotic behavior expected at high frequencies. In order to quantify the error of $\sigma_{\rm rad}$ as a function of M', the following error function is defined:

$$\varepsilon_{M'} = \frac{\sum_{j=1}^{N_{\rm freq}} \left|\sigma_{\rm rad}(f, M'_{i+1}) - \sigma_{\rm rad}(f, M'_i)\right|}{\sum_{j=1}^{N_{\rm freq}} \sigma_{\rm rad}(f, M'_i)}. \quad (11)$$

In Fig. 10 it is shown the convergence error ratio of the radiation efficiency as a function of M'. For $M' = 2$ the error rate is very large. However, for $M' = 63$ the same is less than 0.1%. On the other hand, the convergence as a function of the radius is much faster than the convergence in terms of M'. It is noteworthy that the increase in radius does not influence the computational cost in calculating $\sigma_{\rm rad}$. However, the parameter M has a strong influence on the computational cost,

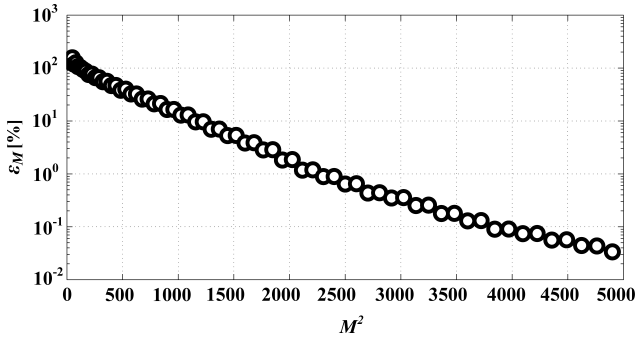

Fig. 10. Convergence error rate (log scale) of radiation efficiency as a function of M'.

because it is directly related to the dimension of $[G]$ (see Eq. (1)). For example, for $M = 20^2$, the size of $[G]$ is 44 MB, while for $M = 70^2$ is 563ḾB. Moreover, the computational time in the former was only 121 seconds, while the later was 1390 seconds. In this work, the current approach was implemented using MATLAB, so that $[G]$ is always a *mat* file. Evidently, it is desirable to obtain a clean curve of radiation efficiency, but the method requires a high computational cost compared to a distorted curve. This may indeed be a great disadvantage compared to other methods that do not exhibit this type of error. However, in the next section it will be shown that taking into account some considerations it will be possible to get reliable curves with a much lower computational cost.

It is very important to understand the nature of the errors that appear in the σ_{rad} curves when using the current approach. From Fig. 9 it is possible to observe that the distortion varies with frequency. In fact, it is possible to quantify the associated error, considering that the radiation efficiency calculated here is a discrete information, because depends of the vibration mode.

On the other hand, one possible way to obtain an approximation of such error, is considering a reference to σ_{rad} as "reasonably acceptable". In this research, the reference are the σ_{rad} values for $M' = 70$. Although such approach is not entirely accurate, the same will be helpful to understand the evolution of the distortion associated when using the current method to calculate the radiation efficiency. Thus, the error as a function of frequency is defined by:

$$\varepsilon_f = \frac{|\sigma_{\text{rad}}(f, M') - \sigma_{\text{rad}}(f, M'_{70})|}{\sigma_{\text{rad}}(f, M'_{70})}. \qquad (12)$$

In Fig. 11 are shown four plots of ε_f for different values of M'. Clearly, the distortion on σ_{rad} depends on the frequency, but not in a simple way. For example, for $M' = 5$ the error increases with frequency and has several abrupt jumps, so it is quite irregular. In general, the error reaches extremely high values, indicating that low values of M' are unsuitable for a reasonable estimate of σ_{rad}. For $M' = 20$, the error remains crescent in the frequency range, but with fewer irregularities to high values, and therefore presents a more uniform behavior, particularly at middle and high frequencies. In the same frequency range we can note that the error is still high, however, the overall error rate is less than that for $M' = 5$.

For $M' = 40$ and $M' = 60$ the error behavior takes a different form: from 40 Hz to 980 Hz the error can be considered constant with frequency. Between 750 Hz and 2400 Hz, the behavior is clearly concave with a maximum value at 1400 Hz. This data set has a well defined trend, and in fact, a polynomial curve fit of order 2 appears to be quite reasonable for representing the error in this region.

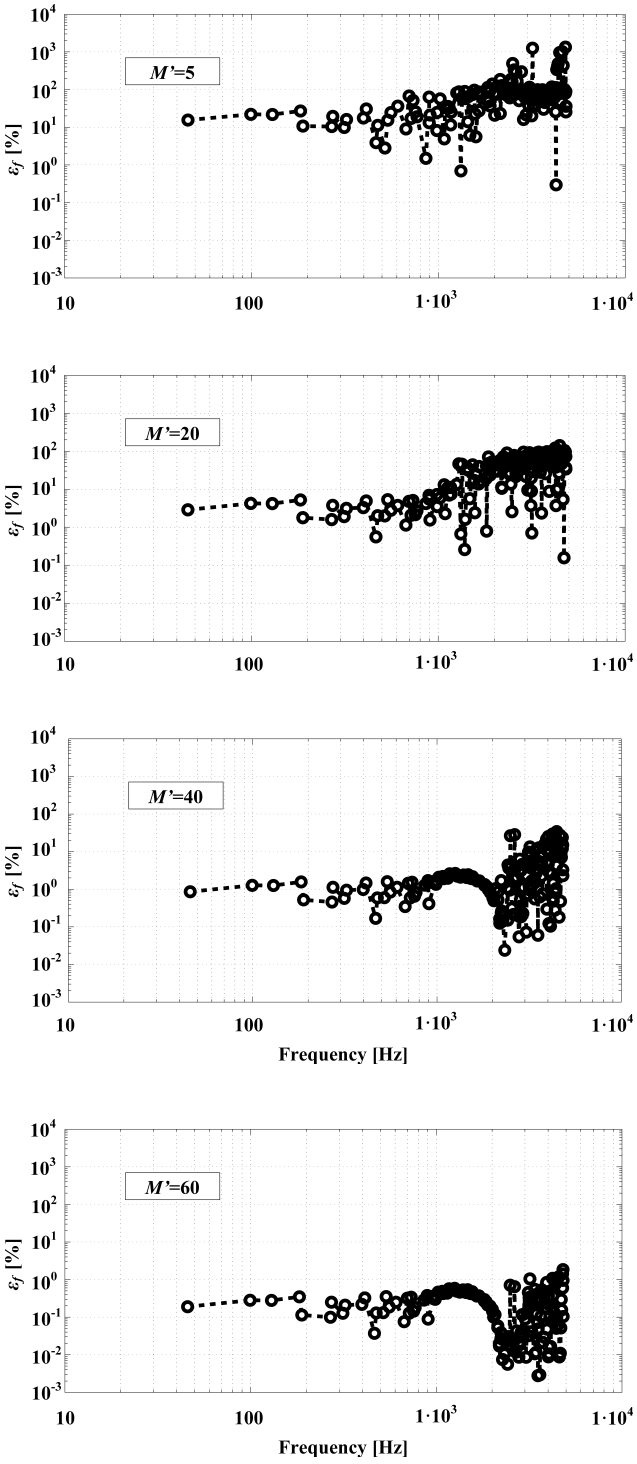

Fig. 11. Error of radiation efficiency with different values of M' as a function of frequency.

For frequencies above 2500 Hz, the behavior of the error is clearly crescent although with high dispersion of data. The information given by the Fig. 11 is valuable, because it indicates that the error generated in σ_{rad} depends on both the frequency and the number of points used in the hemispherical surface. However,

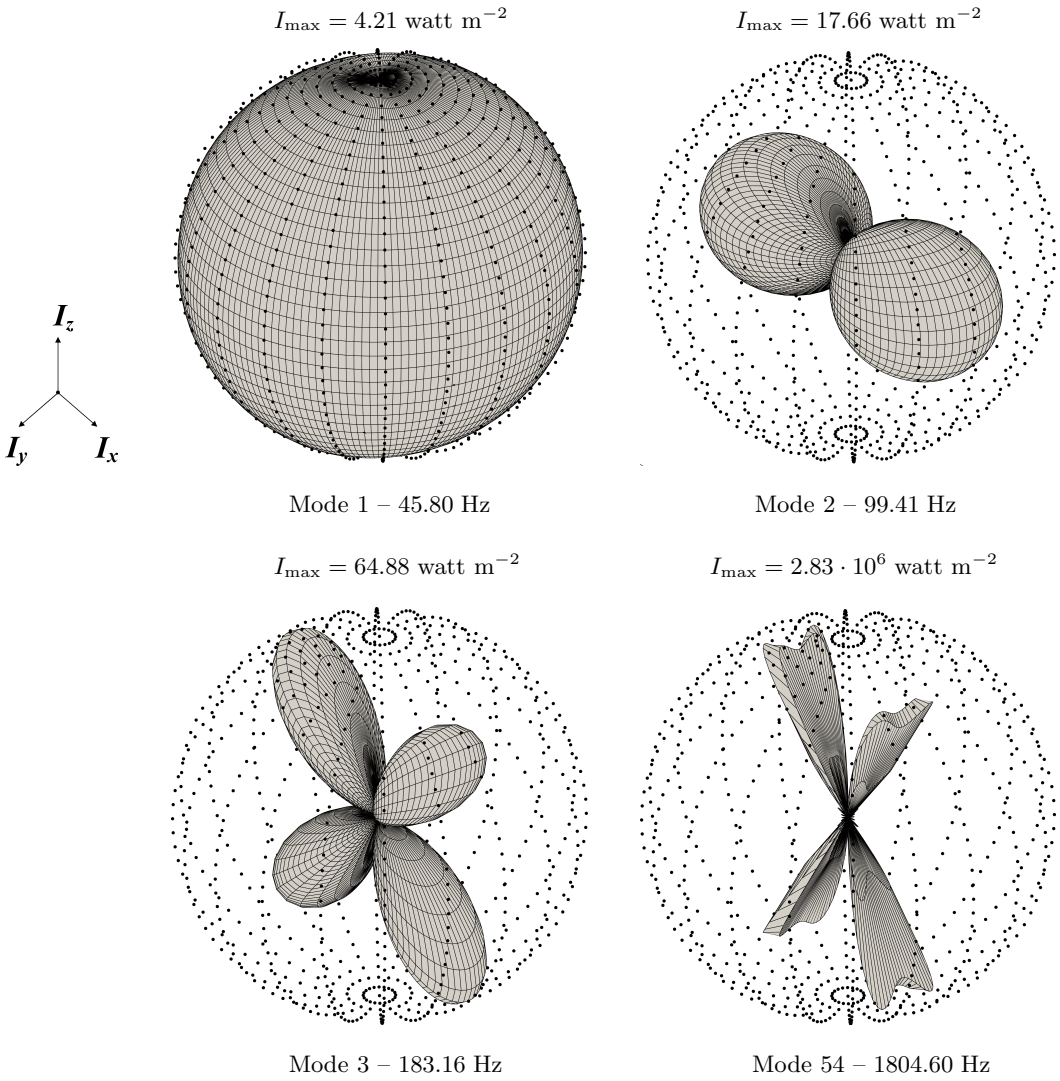

Fig. 12. Acoustic intensity in the far field generated by the vibrating structure surface.

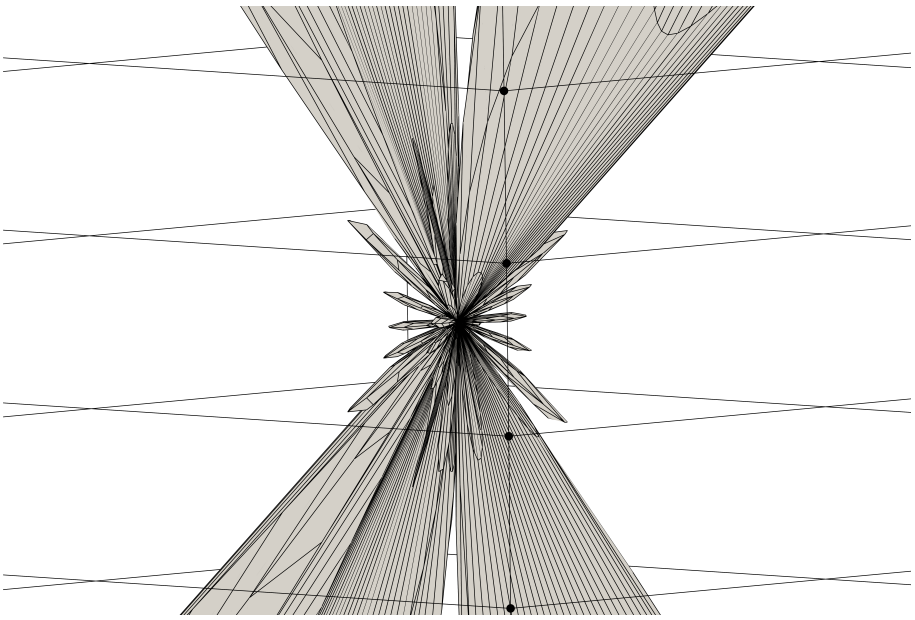

Fig. 13. Acoustic intensity in the far field generated by the vibrating structure surface. Zoom of mode 54.

by itself it is not enough to understand the nature of the error. The concept that can be useful is the *directivity of the source*. In fact, the present methodology to calculate σ_{rad} is based on the far field of the sound pressure generated by the vibrating structure, and therefore, the sound power must also be sensitive to the spatial distribution of sound pressure, i.e. the directivity of the source.

It is interesting to show the directivity patterns for a structural mode of the panel. At high frequencies, the directivity pattern exhibits an important increase in the number of lobes and consequently, the hemisphere should have more points if we need to perform an accurate integration of the acoustic intensity on the surface. In Figs. 12 and 13 it is illustrated the modulus of the acoustic intensity to the far field, for various modes of vibration of the structure considered in this work. Black spots belong to the surface of a sphere with radius equal to the maximum value of the sound intensity modulus, where the spatial discretization is the same as that used for the hemispherical surface of Fig. 2, and is defined similarly to the Eqs. (2), (3). In that sense, it was chosen a complete sphere and not just one hemisphere, in order to have a better spatial visualization of radiation patterns.

The first and second vibration modes are associated to a monopole and dipole, respectively, which are typical radiation patterns for a flat rectangular panel mounted in a infinite baffle according to the literature (Cremer *et al.*, 1988). The spheres of Fig. 12 are formed by 800 points each, which corresponds to the case $M' = 20$. In Fig. 11 it is noted that the error is approximately 2.9% for the first vibration mode, while for the second and fourth modes is 4.2 and 5.2%, respectively. Clearly the error is increased, at least to the first modes, and this can be justified by the directivity, because the directional patterns become more complicated (geometrically) at higher frequencies, so that it is not possible to realize a good integration of the sound intensity over the hemispherical surface using few points. That is the reason why better results are obtained for σ_{rad} for higher values of M'.

Particularly, this is true for the mode 54, which is highly directional and has several minor lobes in different directions (see Fig. 13). Thus, for this case it is clearly noticeable the need of a more refined mesh for the hemispherical surface.

5. Comparison in terms of computational performance

It is very important to evaluate the approach in terms of computational performance. One way to do this is to compare the current method (or G method), with some near field approach, such as the Radiation Impedance Matrix Method (or Z method). In that sense, the sound power can be expressed in the following quadratic matrix formulation introduced by Fahy (Fahy, Gardonio, 2007):

$$\begin{aligned} W_{\text{rad}} &= \frac{S}{2}\text{Re}\{\{v_e\}^H\}\{p_e\}\} \\ &= \frac{S}{2}\text{Re}\{\{v_e\}^H\}[Z]\{v_e\}\}, \\ \{p_e\} &= [Z]\{v_e\}, \\ Z_{rs} &= \frac{j\omega\rho_0 A_e e^{-jkR_{rs}}}{2\pi R_{rs}}, \end{aligned} \tag{13}$$

where $[Z]$ is the Impedance Matrix, which incorporates the point and transfer acoustic impedance terms over the grid of elements that represent the structure, $\{p_e\}$, $\{v_e\}$ are the acoustic pressure and normal velocity vectors, R_{rs} is the distance between the centers of the r-th and s-th elements, S represents the area of the surface and H is the hermitian operator. It should be noted that for $r = s$, there is a singular problem. In this case, it may be useful the following approximation of the Rayleigh integral given by Bai and Tsao to the diagonal terms (Bai, Tsao, 2002):

$$Z_{rr} = \frac{1}{2}\left(k\sqrt{\frac{S}{\pi}}\right)^2 - j\frac{8}{3\pi}\left(k\sqrt{\frac{S}{\pi}}\right). \tag{14}$$

One more time, it will be consider the same structure analyzed in Secs. 3 and 4. Figure 14 shows a comparison in terms of the radiation efficiency. The Z Method may be consider as a "good reference", since this approach is well-known in the literature. Moreover, the results should be reliable, because the calculations are based in the near field data and thus, there are no problems associated with directivity. At high frequencies there are some little perturbations of σ_{rad} (Fig. 14, grey line) but, in general, the curve presents the expected behavior. On the other hand, the

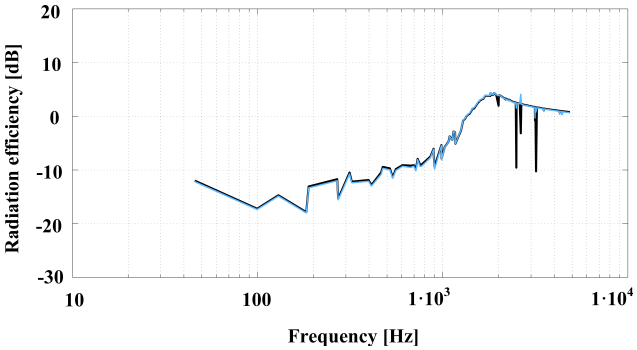

Fig. 14. Radiation efficiency calculated by two methods: Z Method (blue line), G Method (black line).

G Method (blue line) exhibits excellent agreement in almost all of the frequency range. At low and middle frequencies no errors are detected, but important ones are clearly visible above the critical frequency, due to the directivity of the source, which has been indicated by Atalla and Nicolas (1994).

For all simulations the mesh was composed of 8000 elements. That means the dimension of $[Z]$ is 8000×8000. However, the storage of large matrices is computational expensive, and requires high computational resources in terms of RAM memory. In that sense, the symmetry of $[Z]$ may be useful to save memory. Indeed, $[Z]$ can be expressed in terms of an upper triangular matrix, $[Z_U]$, and the diagonal of $[Z]$ as:

$$[Z] = [Z_U] + [Z_U]^{\mathrm{T}} + \mathrm{diag}[Z], \tag{15}$$

where "T" is the transpose operator, and $\mathrm{diag}[Z]$ is the $N \times N$ matrix containing the diagonal elements of $[Z]$. This matrices are computationally less expensive to storage than the full matrix. To this case, the size of $[Z_U]$ was 368 MB and 7205 seconds were required (approximately 2hrs) for the σ_{rad} calculation. To the G case and with $M' = 70$, the size of $[G]$ was 544 MB and 1395 seconds (approximately 23 minutes) were necessary. Thus, it is observed that even when $[Z_U]$ is computationally less expensive, the use of Eq. (13) along with Eq. (15) is much slower than the G Method, possibly due to the matrix operations such as transposition. This operation may be computational expensive for large matrices. Moreover, the multiplication of a matrix by a vector must be performed more than once.

On the other hand, the G Method is very fast, although the size of $[G]$ may cause problems of storage. So, it is desirable to decrease the size of $[G]$ and this is possible by consider small values of M'. However, it was seen in the last section that important errors are associated to σ_{rad} that depends on the value of M'. In that sense, there is concern whether it would be possible to decrease the size of $[G]$ in terms of M' without sacrificing the quality of results, particularly at middle and high frequencies. The CPU times and the sizes of $[G]$ are shown in Table 1, for the four simulations, considering different values of M'. Obviously, increasing M' implies an increase of these computational parameters. In Fig. 15 the corresponding σ_{rad} curves are plotted. As already discussed, it appears that the G Method is computationally expensive at high frequencies, and therefore requires a large number of points in the hemisphere surface (M' larger), in order to reduce the associated error. Figure 16 presents the same cases, but considering the radiation efficiency in frequency bands. Indeed, in this work has been used third octave bands. It is very interesting to compare Fig. 15 and Fig. 16, because even being exactly the same performed simulations, the σ_{rad} curves of Fig. 16 are practically equal, particularly for $M' = 30$, 50 and 70.

Table 1. Computational parameters of G Method for several values of M'.

	$M' = 10$	$M' = 30$	$M' = 50$	$M' = 70$
cpu-time [s]	37	264	715	1393
size $[G]$ [MB]	10.4	101	286	563

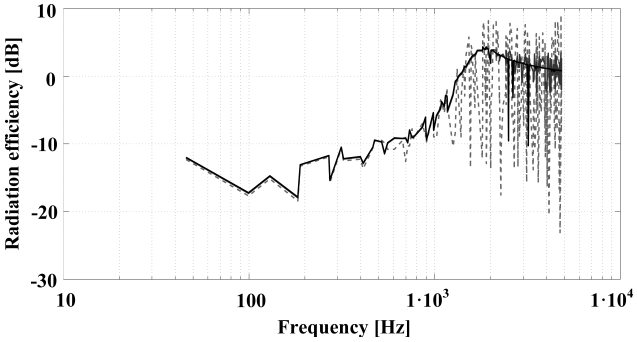

Fig. 15. Radiation efficiency calculated for several values of the parameter M: $M' = 10$ ——— , $M' = 30$ ——— , $M' = 50$ . . . . , $M' = 70$ ——— .

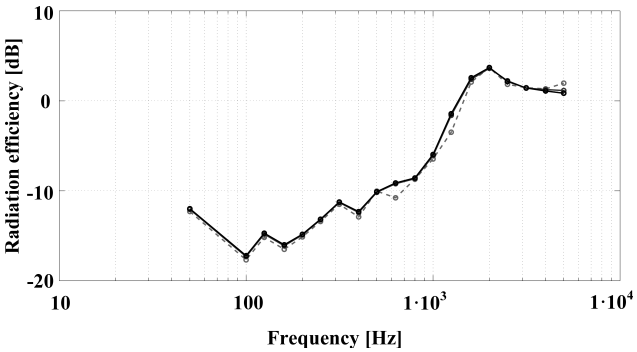

Fig. 16. Radiation efficiency calculated for several values of the parameter M: $M' = 10$ ——— , $M' = 30$ ——— , $M' = 50$ . . . . , $M' = 70$ ——— .

The preceding observation is undoubtedly valuable, since it indicates that *the errors associated with M' can be reduced without greatly increasing M', which is helpful to decrease the computational effort in terms of CPU time and memory size storage*. This means that when considered the analysis in frequency bands, the results can be obtained more faster with the G Method than the Z Method, because $[G]$ it is a $M \times N$ matrix, while $[Z]$ it is a $N \times N$. Indeed, M may be substantially small than N since M can be choice with more "flexibility" (represents the number of points over a hemisphere surface), whereas N represents the number of elements of the panel and therefore, with few possibilities of changes.

The same observations can be derived from a convergence analysis, such as the one illustrated in Fig. 17. Evidently, the frequency band representation of σ_{rad} converges faster than the mode-by-mode representa-

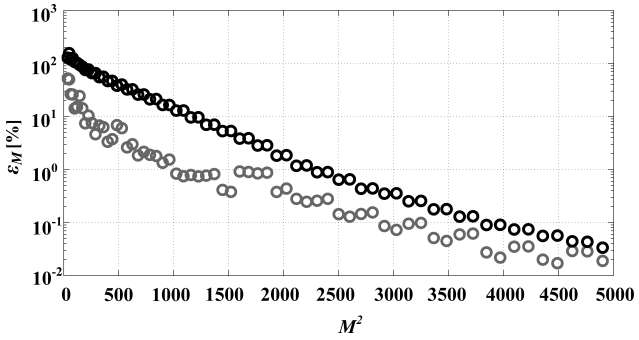

Fig. 17. Convergence error rate (log scale) of radiation efficiency with discretization of the hemispherical surface parameter M': Mode by Mode ——, in frequency bands ——.

tion, allowing obtaining the vibroacoustic information in less time and with less computational resources.

6. Discussion

Regarding numerical methods, any improvement in the accuracy of results implies some type of loss. Indeed, the current method is not the exception, since the advantages of speed and computational effort were obtained by sacrificing the specific information of each mode, and now the radiation efficiency is obtained in frequency bands. This type of representation is not inappropriate and this is particularly true in acoustic and vibration problems.

In that sense, the approach proposed in this work, along with the representation in frequency bands, yields a good representation of radiation efficiency in a wide frequency range.

Although the advantages of using frequency bands are obvious enough (see Fig. 17), it would be appropriate to develop a research to explain, on the basis of underlying physics, why this way of representation entails to the consequences referred above.

Another point of discussion is related to the integration method over the hemispherical surface. Indeed, the current approach was implemented by using a common Riemann summation. Even so, important results have been obtained in this work using such a simple algorithm. However, Figs. 10 and 17 show some fluctuation in the convergence plots, and it is thought to be due to the oddness or evenness of M_θ and M_ϕ (Eqs. (2) and (3)). Perhaps it would be possible to decrease these errors by using a more efficient algorithm such as a Simpson method. In this respect, it is thought that even using a very efficient one on the hemispherical surface, it would be necessary to use a large number of points due to the complexity of the far-field directivity. Thus, it would be interesting to develop and investigation about numerical integration methods over an hemispherical surface along with a more thorough study about the nature of the directivity function.

7. Concluding remarks

A numerical method for estimating the sound power of a baffled planar vibrating structure has been presented. This approach is based on the concepts of acoustic far field and the propagating matrix. Finite element codes were used to calculate the vibrating velocity profile, so that it is possible to estimate the sound power and radiation efficiency of an arbitrary shape. Good agreement was achieved when compared with near field techniques, such as the impedance matrix method (Fahy, Gardonio, 2007) and the Williams-Maynard's method (Williams, Maynard, 1982).

Although the literature review indicates that far field approaches are expensive due to large variations of directivity of the source (Atalla, Nicolas, 1994), in this investigation has been found that this type of approach is computationally more efficient than other methods when the numerical data (in this case the radiation efficiency) is represented in frequency bands. Indeed, it has been shown that this advantage is possible when the number of pressure points in the far field is reduced, enabling to reduce the size of the matrix $[G]$ and without loss of the vibrating velocity information.

Some issues related to this methodology need to be investigated in further researches. For example, although were shown the advantages of using a frequency band representation of the vibroacoustic data, it would be appropriate to explain why this occurs from a mathematical and physical point of view. Also, it would be important to improve the numerical integration over the hemisphere surface along with further study of the directivity function, by considering several types of vibrating structures.

Acknowledgments

Thanks are given to Dr. Fábio Fiates, who shared his valuable PhD Thesis. This work has been financially supported by CAPES/CNPQ.

References

1. Arenas J.P., Ramis J., Alba J. (2010), *Estimation of the sound pressure field of a baffled uniform elliptically shaped transducer*, Appl. Acoust., **71**, 128–133.
2. Atalla N., Nicolas J. (1994), *A new tool for predicting rapidly and rigorously the radiation efficiency of plate-like structures*, J. Acoust. Soc. Am., **95**, 3369–3378.
3. Bai M.R., Tsao M. (2002), *Estimation of sound power of baffled planar sources using radiation matrices*, J. Acoust. Soc. Am., **112**, 876–883.
4. Baumann W.T., Ho F.-S., Robertshaw H.H. (1992), *Active structural acoustic control of broadband disturbances*, J. Acoust. Soc. Am., **92**, 1998–2005.

5. Berkhoff A.P. (2002), *Broadband radiation modes: Estimation and active control*, J. Acoust. Soc. Am., **111**, 1295–1305.
6. Berry A. (1991), *Vibration and acoustic radiation of planar structures, complex immersed in a light fluid or in a heavy fluid*, [in French: *Vibrations et rayonnement acoustique de structures planes, complexes immergées dans un fluide léger ou dans un fluide lourd*], Université de Sherbrooke, Ph.D. Thesis.
7. Borgiotti G.V. (1990), *The power radiated by a vibrating body in an acoustic fluid and its determination from boundary measurements*, J. Acoust. Soc. Am., **88**, 1884–1893.
8. Borgiotti G.V., Jones K.E. (1994), *Frequency independence property of radiation spatial filters*, J. Acoust. Soc. Am., **96**, 3516–3524.
9. Cremer L., Heckl M., Ungar E.E. (1988), *Structure-Borne Sound*, Springer-Verlag, Berlin.
10. Cunefare K.A., Koopmann G.H. (1991), *Global optimum active noise control: Surface and far-field effects*, J. Acoust. Soc. Am., **90**, 365–373.
11. Elliot S.J., Johnson M.E. (1993), *Radiation modes and the active control of sound power*, J. Acoust. Soc. Am., **94**, 2194–2204.
12. Fahy F.J., Gardonio P. (2007), *Sound and Structural Vibration*, Academic Press, Oxford.
13. Fan X., Moros E., Straube W.L. (1997), *Acoustic field prediction for a single planar continuous-wave source using an equivalent phased array method*, J. Acoust. Soc. Am., **102**, 2734–2741.
14. Fiates F. (2003), *Sound radiation of beam-reinforced plates*, [in Portuguese: *Radiação sonora de placas reforçadas por vigas*], Universidade Federal de Santa Catarina, Ph.D. Thesis.
15. Fisher J.M., Blotter J.D., Somerfeldt S.D., Gee K.L. (2012), *Development of a pseudo-uniform structural quantity for use in active structural acoustic control of simply supported plates: An analytical comparison*, J. Acoust. Soc. Am., **131**, 3833–3840.
16. ISO-3745 (2003), *Acoustics – Determination of sound power levels of noise sources – Precision methods for anechoic and semi-anechoic rooms*, Geneva, Switzerland: ISO.
17. Langley R.S. (2007), *Numerical evaluation of the acoustic radiation from planar structures with general baffle conditions using wavelets*, J. Acoust. Soc. Am., **121**, 766–777.
18. Li W.L. (2006), *Vibroacoustic analysis of rectangular plates with elastic rotational edge restraints*, J. Acoust. Soc. Am., **120**, 769–779.
19. Maidanik G. (1962), *Response of Ribbed Panels to Reverberant Acoustic Fields*, J. Acoust. Soc. Am., **34**, 809–826.
20. Mollo C.G., Bernhard R.J. (1989), *Generalised method of predicting optimal performance of active noise controllers*, J. AIAA, **27**, 1473–1478.
21. Naghshineh K., Koopmann G.H., Belegundu A.D. (1992), *Material tailoring of structures to achieve a minimum radiation condition*, J. Acoust. Soc. Am., **92**, 841–855.
22. Naghshineh K., Koopmann G.H. (1993), *Active control of sound power using acoustic basis functions as surface velocity filters*, J. Acoust. Soc. Am., **93**, 2740–2752.
23. Pàmies T., Romeu J., Genescà M., Balastegui A. (2011), *Sound radiation from an aperture in a rectangular enclosure under low modal conditions*, J. Acoust. Soc. Am., **130**, 239–248.
24. Rayleigh L. (1896), *The Theory of Sound*, Dover, 130, New York.
25. Sandman B.E. (1977), *Fluid-loaded vibration of an elastic plate carrying a concentrated mass*, J. Acoust. Soc. Am., **61**, 1503–1510.
26. Wallace C.E. (1972), *Radiation resistance of a rectangular panel*, J. Acoust. Soc. Am., **51**, 946–952.
27. Williams E.G., Maynard J.D. (1982), *Numerical evaluation of the Rayleigh integral for planar radiators using the FFT*, J. Acoust. Soc. Am., **72**, 2020–2030.
28. Zou D., Crocker M.J. (2009), *Sound Power Radiated from Rectangular Plates*, Arch. Acoust., **34**, 1, 25–39.